

Robotic Mapping Using Measurement Likelihood Filtering

John Mullane, Martin D. Adams, Wijerupage Sardha Wijesoma

School of Electrical & Electronic Engineering

Nanyang Technological University

Singapore

john.mullane@pmail.ntu.edu.sg, eadams@ntu.edu.sg, eswwijesoma@ntu.edu.sg

Abstract—The classical occupancy grid formulation requires the use of a priori known measurement likelihoods whose values are typically either assumed, or learned from training data. Furthermore in previous approaches, the likelihoods used to propagate the occupancy map variables are in fact independent of the state of interest and are derived from the spatial uncertainty of the detected point. This allows for the use of a discrete Bayes filter as a solution to the problem, as discrete occupancy measurement likelihoods are used. In this paper, it is firstly shown that once the measurement space is re-defined, theoretically accurate and state dependant measurement likelihoods can be obtained and used in the propagation of the occupancy random variable. The required measurement likelihoods for occupancy filtering are in fact those commonly encountered in both the landmark detection and data association hypotheses decisions. However, the required likelihoods are generally *a priori* unknown as they are a highly non-linear function of the landmark's signal-to-noise ratio and the surrounding environment.

The probabilistic occupancy mapping problem is therefore reformulated as a continuous joint estimation problem where the measurement likelihoods are treated as continuous random states which must be jointly estimated with the map. In particular, this work explicitly considers the sensors detection and false alarm probabilities in the occupancy mapping formulation. A particle solution is proposed which recursively estimates both the posterior on the map and the measurement likelihoods. The ideas presented in this paper are demonstrated in the field robotics domain using a millimeter wave radar sensor and comparisons with previous approaches, using constant discrete measurement likelihoods, are shown. A manually constructed ground-truth map and satellite imagery are also provided for map validation.

Index Terms—Radar target detection, Occupancy grid, Measurement likelihoods

I. INTRODUCTION

Autonomous outdoor navigation is still a very active topic of research due to the presence of unstructured objects and rough terrain in realistic situations. One of the core reasons for failure is the difficulty in the consistent detection and association of landmarks present in the environment. Mobile robot navigation is typically formulated as a dynamic state estimation process where predicted vehicle and landmark locations are fused with sensor readings. Reliable landmark detection from noisy sensor data is critical to the successful convergence of any such algorithm. Most methods are concerned only in the location of detected landmarks, thus the noise in the sensor readings is typically 2 dimensional i.e. in range, r , and bearing, θ . For range/bearing sensors commonly used in robot navigation, such as the polaroid

sonar or SICK laser, the landmark detection algorithm is performed internally resulting in a single (r, θ) output to the *first* signal considered detected. No other information is returned about the world along the bearing angle θ however it is typical, in the case of most sensor models, to assume empty space up to range r [Leonard and Durrant-Whyte, 1990]. This signal may correspond to a landmark or may be a noise or multipath signal, depending on the environmental properties. These ambiguities are typically resolved in the data association stage by applying a threshold to a statistical distance metric, based on the covariance of the predicted and observed landmark locations [Kirubarajan and Bar-Shalom, 2001].

Sensor noise in range/bearing measuring sensors however is in fact 3 dimensional, since an added uncertainty exists in the detection process itself. Most localisation algorithms will disregard this uncertainty and assume an ideal detector, where every detection is treated as a valid landmark and added to the map after passing some heuristic landmark initialisation requirements. Using this assumption, the distribution of the landmark's spatial coordinates can be conveniently modeled with probability density functions (typically Gaussian), where the probabilistic sum under the distribution is unity. That is, complete certainty is assumed that a landmark exists *some-where* within that area, thus readily allowing for numerous stochastic filtering techniques to be applied. For most occupancy grid maps, the occupancy is distributed in a Gaussian manner as a function of the returned range, the intensity of the returned signal is rarely considered, resulting in *discrete* observations of occupancy in each cell. The discrete Bayes filter is then used as a solution, which is possible as it subtly assumes a completely known occupancy measurement model to update the posterior occupancy probability.

For most sensors, users do not have access to the signal detection parameters, however this is not the case for sensors such as the frequency modulated continuous wave (FMCW) radar¹ and certain underwater sonar devices [Ribas et al., 2007] where the output data is a complete signal power profile along the direction of beam projection, without any signal detection being performed. At each range bin, a power value is returned thus giving information at multiple ranges for a single bearing angle. FMCW radar sensors are typically

¹Due to the modulating techniques, a Fast Fourier Transform can be used to return a power value at discrete range increments. Range resolution, beamwidth, and maximum range are dependant on the particular sensor.

applied to outdoor sensing applications as they can operate under various environmental conditions where other sensors will fail. This is due to the radar's ability to penetrate dust, fog, and rain [Brooker et al., 2001].

II. RELATED WORK

In cluttered outdoor or underwater environments where there can be numerous false alarms (incorrectly declared landmarks) and/or outliers (infrequent spurious returns), so called 'landmark management' techniques are often used to identify 'unreliable' landmarks and delete them from the map. This is in order to reduce the possibility of false data association decisions. From the literature, two common methods of identifying true landmarks from noisy measurements are the discrete Bayes filter [Montemerlo et al., 2003], [Thrun, 2003], which propagates a landmark existence variable obtained from a sensor model and the 'geometric landmark track quality' measure [Dissanayake et al., 2001], [Makarov and Durrant-Whyte, 1995] which is a function of the innovation for that landmark. The discrete Bayes filter approach is more commonly used in an occupancy grid framework for map building applications.

Signal processing problems are not new to the field of autonomous mapping and landmark detection but are generally treated in a simplified manner. In the underwater domain, sonars also return a power versus range vector which is difficult to interpret. In his thesis [Williams, 2001], S. Williams outlined a simple landmark detection technique for autonomous navigation in a coral reef environment. The maximum signal to noise ratio exceeding an *a priori* constant threshold is chosen as the point target. Clearly this method of extraction results in a large loss of information, as the power information at all other ranges except that which is declared a landmark is disregarded. This can compromise the amount of information present in the map. In [Majumder, 2001] S. Majumder attempts to overcome this loss by fitting sum of Gaussian probability density functions to the raw sensor data (in the form of a power vs range spectrum), however this represents a likelihood distribution in range of a *single point landmark* which is misleading as the data can be the result of multiple landmarks, leading to the association of non-corresponding landmarks.

In field robotics, standard noise power thresholding² was again used by S. Clark [Clark and Durrant-Whyte, 1998] using an FMCW radar. The range and bearing measurements of the detected point were then propagated through an extended Kalman Filter framework to perform navigation and mapping. The method was shown to work in an environment containing a small number of well separated, highly reflective beacons. The method was extended slightly in [Clark and Dissanayake, 1999] where, *even bounce specularities* were used to extract pose invariant landmarks. Again the environment contained reflective, metallic containers. A. Foessel [Foessel et al.,

2001] also demonstrated radar mapping capability through the use of a log odds approach using a heuristic scoring scheme. Impressive results were produced however, detection statistics were not considered and mathematical justification for the model was also not provided.

This paper further explores the problem of signal detection within a robotics framework to perform mapping. It is shown that by using signal detection theory, the occupancy random variable has a precise (but unknown) measurement likelihood, and that previous occupancy approaches in fact use a theoretically incorrect likelihood which is independent of the state of interest. Furthermore, it is shown that the discrete Bayes filter is no longer applicable to the propagation of this variable, as the measurement likelihood itself is not discrete. A new particle filter based method is therefore developed to estimate the posterior distribution of the occupancy variable and perform map building.

The paper is organized as follows: Section III outlines the general occupancy grid problem, showing how the exact occupancy variable measurement likelihood can be used when signal detection theory is considered. The problems with a discrete Bayes filter solution are also discussed. Section IV presents the problem formulation while section V discusses a particle filter solution to the occupancy variable estimation recursion. Section VI then presents some results of the proposed method using real radar data collected from outdoor field experiments and comparisons with previous approaches as well as images and occupancy maps generated by SICK laser range finders for map validation.

III. THE GRID-BASED ROBOTIC MAPPING PROBLEM

Probabilistic robotic mapping (RM) comprises stochastic methods of estimating the posterior density on the map, when at each time instance, the vehicle trajectory, $X^k = [X_0, \dots, X_k]$, is assumed *a priori* known. The posterior density of interest for the RM problem is therefore,

$$p_{k|k}(M_k|Z^k, X^k).$$

This density encapsulates all the relevant statistical information of the map M_k , where $Z^k = [Z_0, \dots, Z_k]$ denotes the history of all measurements, up to and including the measurement at time k . Each measurement, $Z_k = [z_k^1, \dots, z_k^3]$, with 3 being the number of measurements at time, k . The density can be recursively propagated, with the standard conditional independence assumptions [Thrun et al., 2005], via the well known Bayesian update,

$$p_{k|k}(M_k|Z^k, X^k) = \frac{p(Z_k|M_k, X_k)p_{k|k-1}(M_k|Z^{k-1}, X_k)}{\int p(Z_k|M_k, X_k)p_{k|k-1}(M_k|Z^{k-1}, X_k)dM_k}. \quad (1)$$

Since a static map is commonly assumed,

$$p_{k|k-1}(M_k|Z^{k-1}, X_k) = p_{k-1|k-1}(M_{k-1}|Z^{k-1}, X^{k-1}) \quad (2)$$

²Fixed threshold detection is indeed the optimal detector in the case of spatially uncorrelated and homogenous noise distributions of known moments.

that is, the time update density in the Bayes recursion is simply the posterior density at time $k-1$. Note that in general, a static map assumption does not necessarily imply that eqn.(2) is valid. This is due to occlusions which may result in corrupted segments of M_k , which consequently cannot be observed by the sensor, nor represented by the likelihood $p(Z_k|M_k, X_k)$. To model this added uncertainty, an extended formulation is required with vehicle state dependant Markov Transition matrices, or state dependant detection probabilities incorporated into the measurement likelihood. Although not explicitly formulated in this manner, this observation was considered in the seminal scan-matching paper of Lu and Milios [Lu and Milios, 1997]. Two methods of metric map representation dominate the autonomous robotics community, namely a feature-based map which consists of dimensionally reduced representations of the environment [Smith et al., 1987], and grid-based maps [Elfes, 1989]. The latter grid-based mapping framework is addressed in this paper.

A grid-based map discretises the naturally continuous cartesian *spatial state space* into a fixed number of fixed sized cells. The map is therefore represented by, $M_k = [m_k^1, \dots, m_k^q]$, where q is the number of a priori assigned grid cells, at predefined discrete spatial cartesian coordinates [Moravec and Elfes, 1985], [Grisetti et al., 2007]. As the cartesian location of the i^{th} cell, m_k^i , is *a priori* assigned, the grid-based map state, m_k^i , comprises an *estimate* of the probability of a landmark existing in that discrete cell, at time k . In this paper, this is referred to as the *occupancy state space*, and is the filtering state space of any grid-based RM algorithm. Here $m_k^i \in \Theta$, with the constraint,

$$\sum_{\theta \in \Theta} \theta = 1. \quad (3)$$

The set Θ can consist of an arbitrary number of hypotheses but usually contains $\{O, E\}$ in the case of a Bayesian approach [Thrun, 2003] and $\{O, E, U\}$ in the case of a Dempster-Shafer approach [Mullane et al., 2006], where O, E, U represent ‘Occupied’, ‘Empty’ and ‘Unknown’ respectively. In this work, the classical Bayesian approach is examined, and M_k then represents the estimate of Occupancy in each cell at time, k . The Emptiness estimate is denoted, $\bar{M}_k = [\bar{m}_k^1, \dots, \bar{m}_k^q]$. The *true* state of the i^{th} cell is denoted, m^i , for occupied, and \bar{m}^i for empty.

The most popular method of evaluating the recursion of eqn.(1) is by modeling the map M_k as a zero order Markov Random field so that each occupancy state, m_k^i can be independently estimated, i.e.,

$$p_{k|k}(M_k|Z^k, X_k) = \prod_{i=1}^{i=q} p_{k|k}(m_k^i|Z^k, X_k).$$

and the update becomes,

$$p_{k|k}(M_k|Z^k, X^k) = \prod_{j=1, i=1}^{j=q, i=q} \frac{p(z_k^j|m_k^i, X_k)p_{k|k-1}(m_k^i|z^{j,k-1}, X^{k-1})}{\int p(z_k^j|m_k^i, X_k)p_{k|k-1}(m_k^i|z^{j,k-1}, X^{k-1})dm_k^i}. \quad (4)$$

Note that for the grid-based RM problem, the number of measurements, z , equals the number of map cells, q . This is because map cells which are not observed (do not interact with sensor beam), are assigned a dummy, non-informative measurement³. Furthermore, since the trajectory, X^k , is assumed known, the map cell-measurement correspondence is assumed known and thus $i=j \quad \forall i=[1, \dots, q]$.

The RM state space filtering problem can then be written as,

$$M_k = M_{k-1} \quad (5)$$

$$Z_k = h(M_k) + V_k \quad (6)$$

which indicates a static time-update and where the measurement is a function $h(\cdot)$ of the state, with V_k being sampled from an assumed *a priori* known noise distribution. Recall that the state in the grid-based RM problem is an estimate of the existence of a landmark at a given discrete location, i.e filtering in the occupancy state space.

A. Grid-Based RM with Range Measurements

This section details the standard method of evaluating the recursion of eqn.(4). For clarity of exposition, the case of the single map cell, m^i , is outlined with the i, j cell and measurement indices being discarded. Since the trajectory, X^k , is assumed known, it is also discarded from the density functions. The measurement likelihood may therefore be written as, $p(z_k|m_k)$, and assuming it to be discrete, it can be shown that [Thrun, 2003]

$$\log \frac{P(m_k|z^k)}{1 - P(m_k|z^k)} = \log \frac{P(m_k|z_k)}{1 - P(m_k|z_k)} + \log \frac{1 - P(m_0)}{P(m_0)} + \log \frac{P(m_{k-1}|z^{k-1})}{1 - P(m_{k-1}|z^{k-1})} \quad (7)$$

where m_0 is the initial estimate on landmark occupancy in the given cell and is typically set at 0.5 [Moravec and Elfes, 1985]. Note that $P(m_k|z_k)$ inversely maps from the measurement at time k to the occupancy state, m_k . These so called ‘inverse’ models are also required by Dempsters update rule,

$$m(\theta_3) = \frac{\sum_{\theta_1 \cap \theta_2 = \theta_3} m_z(\theta_1)m_m(\theta_2)}{1 - \sum_{\theta_1 \cap \theta_2 = \emptyset} m_z(\theta_1)m_m(\theta_2)}. \quad (8)$$

Here $m_z(\cdot)$ and $m_m(\cdot)$ represent *mass functions* respectively containing the sensor and prior map evidences in support of each hypothesis, $\{\theta_1, \theta_2, \theta_3\}$ that is, a direct mapping from the sensor measurement to the evidence in support of each hypothesis. However, these approaches require ‘intuitive’ models which lack mathematical justification and are contrary to the way in which range measuring sensors operate. This may result in inconsistent maps as shown in [Thrun, 2003].

Approaches using the ‘forward’ sensor model, $p(z_k|m_k)$, are also proposed [Konolige, 1997], [Thrun, 2003]. These

³Note that in the commonly considered *spatial state space* feature-based approaches [Smith et al., 1987], the number of measurements typically *does not* equal the number of elements in the map state.

more theoretically founded approaches attempt to obtain the likelihood of a measurement, given the state m_k . For previous grid-based RM algorithms, the measurement z_k , used for the evaluation of the likelihood, $p(z_k|m_k)$, comprises a *range reading* reported by the exteroceptive range measurement unit, assuming a 1D reading. A range reading corrupted by a Gaussian distributed noise signal of variance, σ^2 , results in a measurement likelihood,

$$P(z_k|m_k) = \frac{1}{\sqrt{2\pi\sigma^2}} e^{-\frac{(z_k-r)^2}{2\sigma^2}}. \quad (9)$$

where r is the true range to the cell. When considering the spatial state, i.e. the location of a given cell m , the measurement equation for the likelihood of eqn.(9) becomes,

$$z_k = h(m, X_k) + v_k \quad (10)$$

where $v_k \sim \mathcal{N}(0, \sigma^2)$ and h is a function relating the spatial state of m , to the range reading, z_k . However, for the grid-based RM problem, since the spatial state space is *a priori* discretised into cells of fixed location, filtering occurs in the occupancy state space. Previous approaches use a discrete interpretation of the likelihood of eqn.(9), and use the evaluation of the likelihood at discrete locations as the occupancy measurement, as depicted in figure 1.

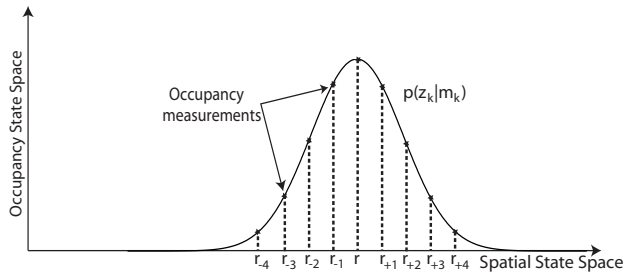


Fig. 1. This figure shows the indirect generation of occupancy measurements from standard range-based algorithms. The evaluation of the Gaussian range likelihood in the surrounding discrete cells with spatial states, r_{-4}, \dots, r_{+4} , are used as occupancy measurements.

From an occupancy state-space perspective, taking the arbitrary case of the range reading reported by the sensor to be $z_k = r_{-2}$, the resulting occupancy measurement becomes,

$$\frac{1}{\sqrt{2\pi\sigma^2}} e^{-\frac{(r_{-2}-r)^2}{2\sigma^2}}.$$

This measurement is a function of the range reading, r_{-2} , and the range measurement noise, σ^2 . However, with respect to the filtering state of interest, m_k , it can be seen that such a measurement has no dependence on the occupancy state. Therefore, this shows that range-based approaches adopt a *state-independent* measurement for propagation of the occupancy state estimate. Furthermore, the occupancy measurement is discrete, which allows for the subsequent discrete Bayes filter implementation proposed in the literature [Konolige, 1997], [Thrun, 2003], [Moravec and Elfes, 1985].

The range at which a sensor reports the presence of a landmark can be used in the filtering of its *spatial* estimate.

However, whilst this may be correlated with the sensor's ability to correctly detect the landmark, the reported range at which the landmark is hypothesised to exist does not provide a measurement of m (the occupancy state) but only a measurement of its location. To correctly formulate the grid-based RM problem from a Bayesian perspective, and have a truly state dependant measurement, the measurement, z_k , should be re-defined as a binary set with $z_k \in \{Detection, No\ Detection\}$. Therefore, through using a range reading as the measurement, previous occupancy sensor models subtly assume complete knowledge of the sensors' detection characteristics, namely $p(z_k|m)$ (probability of detection) and $p(z_k|\bar{m})$ (probability of false alarm), and the occupancy measurements become discrete. That is $p(z_k|m)$ (and $p(z_k|\bar{m})$) are assumed completely known. Note this is typically the case for most likelihood calculations including data association [Wijesoma et al., 2006] and particle filter SLAM solutions [Grisetti et al., 2007], where landmark detection likelihoods are assumed known or ignored completely. The following section outlines the reformulation of the discrete grid-based RM filter.

B. Grid-Based RM with Detection Measurements

Once the occupancy measurement, z_k , is defined in detection space rather than range-bearing space, the measurement likelihoods (for both detection and non-detection) become real signal processing parameters. A simple expansion of the occupancy posterior where the measurements are detections and non-detections, shows how the occupancy measurement likelihoods can be obtained when the signal processing stage is considered. Consider the probability of occupancy given a history of measurements,

$$P(m_k|z^k).$$

The measurement history z^k is now considered to be a series of binary hypothesis decisions on the presence or absence of a landmark (derived through some function of the measured signal intensity) given by the measurement model. Thus each measurement, z_k , is the output of a likelihood ratio test and can be denoted D if a detection was made, or \bar{D} if no detection was made. We can then expand about both measurement hypotheses to get,

$$P(m_k|z_k=D, z^{k-1}) = \gamma_D^{-1} P(z_k=D|m_k) P(m_k|z^{k-1}) \quad (11)$$

$$\gamma_D = P(z_k=D|m_k) P(m_k|z^{k-1}) + P(z_k=D|\bar{m}_k) P(\bar{m}_k|z^{k-1}) \quad (12)$$

$$P(m_k|z_k=\bar{D}, z^{k-1}) = \gamma_{\bar{D}}^{-1} P(z_k=\bar{D}|m_k) P(m_k|z^{k-1}) \quad (13)$$

$$\gamma_{\bar{D}} = P(z_k=\bar{D}|m_k) P(m_k|z^{k-1}) + P(z_k=\bar{D}|\bar{m}_k) P(\bar{m}_k|z^{k-1}) \quad (14)$$

These equations calculate, in closed form, a statistically correct posterior of the occupancy random variable, where the measurement likelihoods $P(z_k=D|m_k)$, $P(z_k=D|\bar{m}_k)$, $P(z_k=\bar{D}|m_k)$ and $P(z_k=\bar{D}|\bar{m}_k)$ are those frequently

encountered in landmark detection algorithms. A graphical representation of the landmark detection hypothesis is shown in figure 2 where,

- $\mathcal{H}_{\bar{m}}$: no landmark signal present

$$s^i \sim p(s|\bar{m}, \Omega_{\bar{m}})$$

- \mathcal{H}_m : landmark signal present

$$s^i \sim p(s|m, \Omega_m)$$

Here, s^i is the power intensity measurement (i.e. a sample) by the sensor, $p(s|m, \Omega_m)$ and $p(s|\bar{m}, \Omega_{\bar{m}})$ represent the received signal fluctuation densities under both landmark presence, m , and landmark absence, \bar{m} , respectively and are further discussed in section IV-D. A likelihood ratio is then defined by [Kay, 1998],

$$L(s) = \frac{p(s|m, \Omega_m)}{p(s|\bar{m}, \Omega_{\bar{m}})} \quad (15)$$

and,

$$z_k = \begin{cases} \text{D} & \text{if } L(s) \geq T \\ \bar{\text{D}} & \text{otherwise.} \end{cases}$$

The four probabilities present in the detection hypothesis problem, which are also required by eqns. (11) and (13), are typically referred to as,

$P(z_k=\text{D}|m)$ – Landmark detection likelihood (DL)

$P(z_k=\text{D}|\bar{m})$ – False alarm likelihood (FAL)

$P(z_k=\bar{\text{D}}|m)$ – Missed detection likelihood (MDL)

$P(z_k=\bar{\text{D}}|\bar{m})$ – “Noise” detection likelihood (NDL).

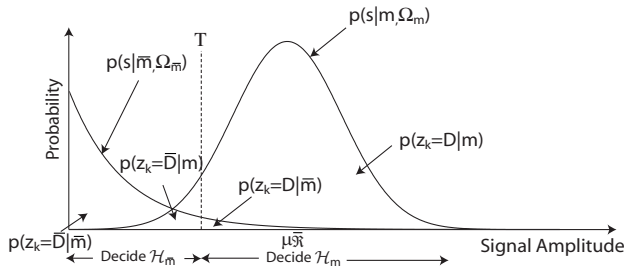


Fig. 2. A graphical representation of the received signal classification problem in a given map cell at time k . T represents the decision threshold, μ is the mean noise power and $\bar{\mathfrak{R}}$ is the mean landmark signal-to-noise ratio. The hypothesis decisions are $\mathcal{H}_{\bar{m}}$: Landmark absent, and \mathcal{H}_m : Landmark present. The measurement likelihoods required to calculate the posterior probability of occupancy are also indicated.

As a result of this subtlety, previous occupancy sensor models typically assume complete knowledge of the sensors’ detection characteristics (detection and false alarm likelihoods), and the occupancy measurements become discrete. The signal processing and measurement intensity information that may be available, are usually ignored. Consequently, this assumption allows for each cell to contain a discrete occupancy measurement which can be updated using the discrete log-odds equation (or Dempsters equation in the case

of evidential measurements). This is in contrast to the landmarks’ *spatial estimates* which use continuous measurement likelihoods and are propagated in a Kalman or particle filter framework.

Given a binary measurement space, discrete measurement likelihoods can be used to calculate the occupancy posterior, through the update equations (11) and (13) which in turn require completely known measurement likelihoods. However, these likelihoods can generally only be calculated exactly when two *a priori* assumptions are made, these are - a *known* mean landmark signal to noise ratio (SNR), $\bar{\mathfrak{R}}$, and *known* landmark power fluctuation likelihood, $p(s|m, \Omega_m)$ [Gandhi and Kassam, 1989]. Under the further assumption of identical and independently distributed (IID) noise power samples, a suitable power threshold can be calculated which will exactly obtain the theoretically derived measurement (and hence occupancy) likelihoods. In this case, the measurements required to calculate the posterior occupancy probability, $P(m_k|z^k)$, are deterministic and a discrete Bayes filter implementation is valid.

However, when these assumptions are relaxed (the primary assumption being the known $\bar{\mathfrak{R}}$), the above measurement likelihoods become continuous and thus the propagation of the occupancy random variable estimate must be carried out using continuous filtering methods (EKF, Particle Filter) as opposed to a discrete filter. As the measurement likelihoods are two complimentary sets, $\{P(z_k=\text{D}|m_k), P(z_k=\bar{\text{D}}|m_k)\}$ and $\{P(z_k=\text{D}|\bar{m}_k), P(z_k=\bar{\text{D}}|\bar{m}_k)\}$, only one likelihood from each set needs to be estimated. Furthermore a discrete filtering approach, which disregards the uncertainty of the measurement likelihood estimate, will equally weight both the measurement and the prior as they are considered to have equal covariances. Occupancy measurements are in fact highly correlated with the vehicle location and structure of the environment, and should not be treated equally. For example, specular reflections are likely to occur at high angles of incidences, and clutter free observations should be treated with greater confidence than those with interfering signals.

C. Detection vs. Range Measurement Models

In this section, the occupancy posterior is propagated for a set of simulated data, illustrating that optimal performance (in terms of estimating the correct number of landmarks) can be achieved when the *actual* measurement likelihoods are used, as opposed to *a priori* assigned values as is typically done in autonomous mapping algorithms. Figure 3 shows a simulated data set with the resulting detection matrix after the application of the detection algorithm. A landmark exists in range bin 11, with other cells empty. The fluctuating signal models the change in power from a landmark with changing vehicle pose. The signal amplitude in empty cells fluctuates according to an assumed noise model (in this case an exponential model). In this example, the false alarm likelihood is set high at 0.1, due to the small sample window (21x20 cells) to ensure some false alarms fall within the surveillance region.

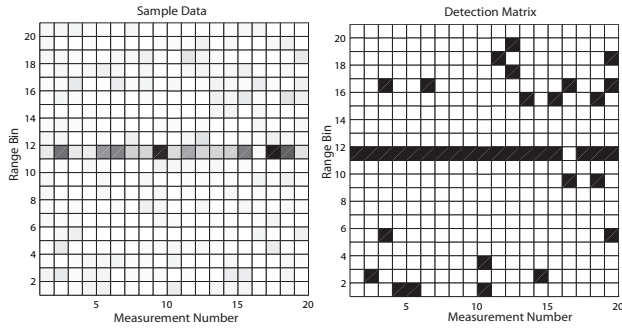


Fig. 3. Sample data and the resulting detection matrix. Note numerous false alarms within the surveillance region as the false alarm likelihood is set to 0.1. For the simulated sample data, the darker the shade of gray, the higher the measured power intensity in that range bin. The detection matrix output shows black for $z_k=\bar{D}$ in that cell and white for $z_k=\bar{D}$.

Using eqns.(11) and (13), the occupancy posterior at each time step is evaluated. Both the range measurement approach and detection measurement approach are compared in this simulated test. Both methods use the detection sequence depicted in figure 3, however the values of the measurement likelihoods are different. The true likelihoods for this sample set (obtained theoretically from the detection algorithm) are $DL = 0.80663$ and $FAL = 0.1$. Using the range measurement model outlined in section III-A [Thrun, 2003] [Konolige, 1997], detection measurement likelihoods are essentially *a priori* assumed and the statistics of the detection algorithm used are ignored. The results in figure 4 show the estimated number of landmarks in the region after 20 measurement updates, where cells with an occupancy probability greater than 0.51 are deemed occupied, and cells with values less than 0.49 are deemed empty.

The figure on the left plots the results from the detection measurement model, using the theoretically true false alarm likelihood and varying the detection likelihood whilst the figure on the right uses the true detection likelihood and varies the false alarm likelihood. Also plotted on both graphs is the estimated number of landmarks from the range measurement model. As the range measurement model does not consider the statistics of the detection algorithm, the estimated number of landmarks in the region remains at 8 for each test as can be seen in the figure. This is due to overly pessimistic *a priori* assignment of the likelihoods (from the Gaussian model of equation 9) the estimated number of landmarks far exceeds the true number. Naturally this value can be tuned or scaled to improve mapping performance for a particular case, however with multiple landmarks having varying measurement likelihoods, optimal performance cannot be obtained.

For the detection measurement model, where the detection likelihoods (independent of range) are used, the values of the likelihoods are varied from 0→1 (plotted along the x-axis) for each test. Note there is large error at low assumed detection likelihoods and high estimated false alarm likelihoods, however as the assumed likelihoods approach the true value, the

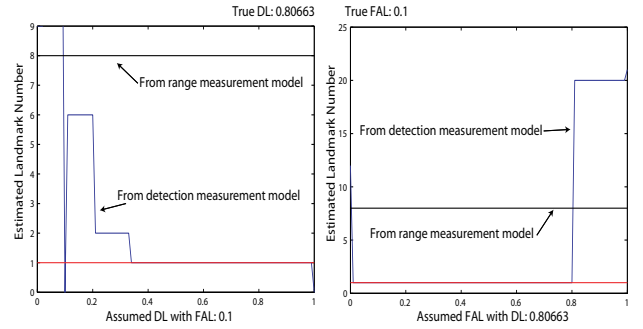


Fig. 4. Comparison of the estimated number of landmarks in the data set after 20 updates using the range measurement model, and the detection measurement model where the true number of landmarks is one. As the range measurement model ignores the statistics of the detection algorithm, a priori assignment may cause inaccuracies. The figure also plots the sensitivity of the occupancy propagation equations to incorrect measurement likelihood estimates.

estimated landmark number converges on the true case (i.e. one landmark present). Thus, as optimal performance can be achieved by having the actual measurement likelihoods, these (state dependant) likelihoods must be jointly estimated with the occupancy posterior.

IV. MAPPING WITH UNKNOWN MEASUREMENT LIKELIHOODS: PROBLEM FORMULATION

This section outlines the proposed algorithm to jointly estimate both the occupancy random variable and the corresponding measurement likelihoods.

A. Data Format

From a radar perspective, the environment can be considered to consist of an unknown number of spatially distributed signal pdfs of both unknown distribution with unknown moments. Figure 2 previously illustrated a noise signal pdf in a given cell, $p(s|\bar{m}, \Omega_{\bar{m}})$, and a landmark signal pdf, $p(s|m, \Omega_m)$. A single sensor sweep therefore acquires samples from these underlying environmental pdfs and returns them in the form of a power-range spectrum at each bearing angle. The data in a single spectrum then contains R samples at discrete range increments (0.25m in this case) along each bearing angle. The data is generally modeled by an R dimensional joint pdf,

$$f_{S_1, \dots, S_R}(s_1, \dots, s_R)$$

where $[s_1, \dots, s_R]$ are R individual samples from (assumed independent) signal pdfs observed by the sensor. Each range at which an intensity sample is acquired by the sensor is referred to as a *range bin*. Thus f_{S_1, \dots, S_R} represent the intensity pdf in each range bin. An example of such a spectrum, collected from an outdoor field test, can be seen in figure 5. A complete scan therefore contains spectra at bearing angles $\{\phi_1, \dots, \phi_{|\Phi|}\} \in \Phi$ and the complete set of measurement samples can be denoted, \mathbf{s}_R^Φ . As before, let $p(s_r|m, \Omega_m)$ be the landmark signal pdf and $p(s_r|\bar{m}, \Omega_{\bar{m}})$ be the noise signal pdf, in the r_{th} range bin where Ω_m and $\Omega_{\bar{m}}$

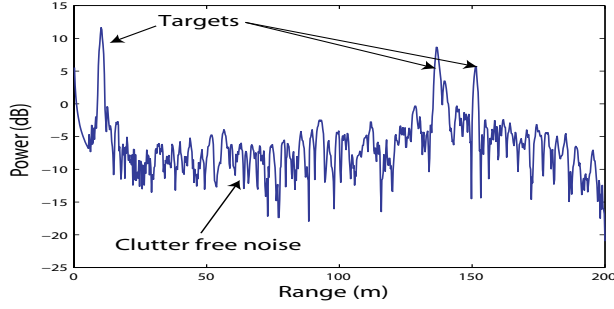


Fig. 5. A sample spectrum, from a frequency modulated continuous wave radar, containing a single signal sample, s_r^i , from each of the R range bins for a single sensor bearing angle. The signal samples are assumed independent. Depending on the presence or absence of a landmark, each sample is $s_r^i \sim p(s_r|m, \Omega_m)$ or $s_r^i \sim p(s_r|\bar{m}, \Omega_{\bar{m}})$ respectively.

are the unknown distribution moments. The noise samples, $s_r^i \sim p(s_r|\bar{m}, \Omega_{\bar{m}})$, are assumed IID, $\forall r \in [1, \dots, R]$, and the moments of $p(s_r|m, \Omega_m)$ are a function of the landmark's mean SNR, $\bar{\mathfrak{R}}$. The spatial distributions are typically modeled by point spread Gaussian functions using the sensor's range and bearing covariances. Adaptive threshold techniques are common in radar signal processing, which use noise samples from surrounding sliding windows to generate a noise estimate and set the threshold, T seen in figure 2 [Gandhi and Kassam, 1989].

B. Mapping Algorithm Overview

Figure 6 shows a block diagram of the estimation problem under consideration. A single power-range spectrum, $\mathbf{s}_R^{\phi_1}$, is considered here which can then be easily generalised to model the complete 360° set of measurements, \mathbf{s}_R^{Φ} . The system input is the true map state, $M = [m^1, \dots, m^R]$, which is a vector of R binary numbers indicating the presence, $m^r = 1$ (also denoted m), or absence, $m^r = 0$, (also denoted \bar{m}) of a landmark in each range bin. The corresponding $\bar{\mathfrak{R}}$, for each landmark is also required, as are modeled in the vector of measurement likelihoods, $\Lambda = [\lambda^1, \dots, \lambda^R]$. The sensor model block then uses the landmarks range, $\bar{\mathfrak{R}}$, and $p(s_r|m, \Omega_m)$ to generate a noise free power-range spectrum, which is in turn corrupted by noise samples taken from $p(s_r|\bar{m}, \Omega_{\bar{m}}) \forall r$ to construct $S(M)$ (for example, figure 5), the collection of power samples comprising a sensor scan. Note that unlike most filtering formulations which assume an *a priori* known noise distribution and moments, here the moments remain *unknown* and must be locally estimated.

C. Constant False Alarm Rate (CFAR) Detector

This block contains the signal detection algorithm which has a constant false alarm rate property. Its input is $S(M)$, and its output, $Z_k = [z_k^1, \dots, z_k^R]$, is a vector of R binary hypotheses, with $z_k^r \in \{D, \bar{D}\}$. Using the assumed noise model (with unknown moments), $p(s_r|\bar{m}, \Omega_{\bar{m}})$, sliding window techniques are used to generate a local estimate of the noise

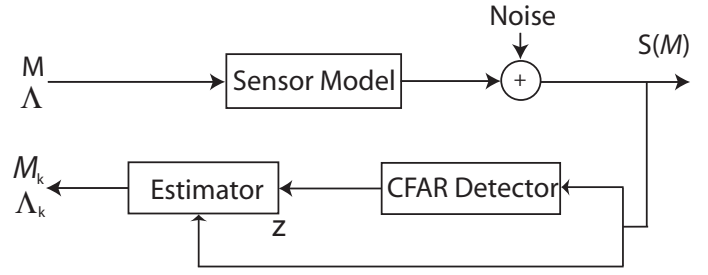


Fig. 6. A block diagram of the proposed algorithm. The aim is to estimate the posterior on the occupancy vector, M . This however requires estimates of the measurement likelihoods $\hat{\Lambda}$. Note the additive noise in radar signal processing is typically non-Gaussian.

distributions moments in each range bin. These are then used in the likelihood ratio test of eqn.(15) to generate the D or \bar{D} hypothesis decision. A more in-depth explanation of this block can be seen in [Mullane et al., 2007].

D. Estimator

The estimation problem is therefore to evaluate the joint likelihood on the occupancy and measurement likelihood random variables at each time k ,

$$p(m_k, \lambda_k | z^k)$$

where the measurement, z^k consists of a history of all raw measurements, and λ , contains the measurement likelihoods (detection and non-detection). This can be expanded to,

$$p(m_k, \lambda_k | z^k) = p(m_k | \lambda_k, z^k) p(\lambda_k | z^k) \quad (16)$$

Since occupancy is a discrete binary random variable,

$$p(m_k = 0 | \lambda_k, z^k) = 1 - p(m_k = 1 | \lambda_k, z^k). \quad (17)$$

As previously stated, λ contains both the detection and non-detection likelihoods, however,

$$\begin{aligned} p(\lambda=D|m=1, z^k) &= P_d \\ p(\lambda=D|m=0, z^k) &= P_{fa} \\ p(\lambda=\bar{D}|m=1, z^k) &= 1 - P_d \\ p(\lambda=\bar{D}|m=0, z^k) &= 1 - P_{fa} \end{aligned}$$

representing a complimentary set of measurement likelihoods. Thus we only need maintain an estimate of $p(\lambda=D|z^k)$ which will be denoted $p(\lambda_k|z^k)$ unless explicitly stated otherwise, whose true value is $p(\lambda|z^k) \in \{P_{fa}, \dots, 1\}$.

As the vehicle traverses the environment, landmarks may randomly appear/disappear in the data due to occlusions as well as falling in and out of the sensors' perception field. Contrary to standard occupancy grid mapping algorithms, a *non-static* time update is used here (i.e. $p(m_k|m_{k-1}, z^{k-1}) \neq p(m_{k-1}|z^{k-1})$). That is, cells can randomly change from occupied to empty or vice-versa during vehicle motion. Thus the process is modeled as a Hidden Markov Model (HMM) where the transition matrix is given by,

$$\Pi = \begin{bmatrix} P_{oo} & P_{eo} \\ P_{oe} & P_{ee} \end{bmatrix}.$$

P_{oo} is the probability of an occupied cell remaining occupied (a stationary landmark remaining within the sensors field of view), P_{eo} being the probability of an empty cell becoming occupied (possibly due to occlusion effects) with P_{oe} being the opposite. P_{ee} is the probability of an empty cell remaining empty. Using Bayes rule on the first term of eqn.(16) we get,

$$p(m_k|\lambda_k, z^k) \propto p(\lambda_k, z_k|m')p(m'|z^{k-1}) \quad (18)$$

where m' is the predicted occupancy obtained from the Markov transition matrix. As λ_k is not dependant the occupancy variable,

$$p(m_k|\lambda_k, z^k) \propto \lambda_k p(z_k|m')p(m'|z^{k-1}) \quad (19)$$

The second term of 16 is a sensor specific representation of the detection likelihood density where a detection may mean range readings in terms of laser, sonar and radar sensors, or feature detections if feature extraction methods are applied to the raw sensor data. As this work uses a radar sensor the density is obtained from examination of CFAR detection theory [Rohling and Mende, 1996].

$$\lambda_k = f(S(M)) \quad (20)$$

where $f(\cdot)$ is a non-linear function of the raw data incorporating signal detection theory. As discussed previously in section IV-A, the measurement data $S(M)$ is assumed to consist of a vector of R consecutive (in time or range) independent signal intensity measurements, s_r , for each bearing angle, shown previously in figure 5. A priori signal distribution assumptions are made on both $p(s_r|m, \Omega_m)$ and $p(s_r|\bar{m}, \Omega_{\bar{m}}) \forall r \in [1 \dots R]$, where the distribution moments Ω_m and $\Omega_{\bar{m}}$ are generally assumed unknown and must be estimated using the signal intensity information. To make an estimate of λ , we must first estimate the mean SNR, $\bar{\mathfrak{R}}$. Taking the measured intensity in bin r , $\{s_r|m\}$, as the signal + noise measurement (assuming the existence of a landmark), we must therefore estimate the local noise intensity at that bin to generate an SNR estimate. Using leading and lagging windows, W intensity measurements are used to generate this estimate. From the signal detection literature [Gandhi and Kassam, 1989], there are numerous adaptive methods of generating local estimates of the unknown noise distribution parameters. Whilst most signal processing literature considers the probability of detection for landmarks of *known* SNR, this work requires λ to be estimated from the measured intensity information using an assumed distribution $p(s|\Omega_m, m)$, but with an *unknown* mean SNR. Thus, given an estimate of the local noise intensity in bin r , $\{s_r|\bar{m}\}$, generated by the detector, $\bar{\mathfrak{R}}_r$ can be estimated as,

$$\bar{\mathfrak{R}}_r = \frac{\{s_r|m\} - \{s_r|\bar{m}\}}{\{s_r|\bar{m}\}}. \quad (21)$$

An ordered-statistics approach [Rohling, 1983], which is adopted in this work, has been shown to be most robust in situations of high clutter and multi-landmark situations, as is commonly encountered in a field robotics environment. Under certain distribution assumptions, using an ordered statistic

noise estimate, closed form solutions exist for λ [Rohling and Mende, 1996],

$$\lambda = \left(1 + \frac{T_r\{s_r|\bar{m}\}}{1 + \bar{\mathfrak{R}}_r}\right)^{-W} \quad (22)$$

with,

$$p(s|\Omega_{\bar{m}} = \mu, \bar{m}) = \frac{1}{\mu} \exp(-s/\mu)$$

$$p(s|\Omega_m = \{\mu, \mathfrak{R}\}, m) = \frac{1}{\mu} \exp((-s/\mu) + \mathfrak{R}) I_0\left(2\sqrt{\frac{\mathfrak{R}s}{\mu}}\right)$$

$$p(\mathfrak{R}|\bar{\mathfrak{R}}) = \frac{2\bar{\mathfrak{R}}}{\mathfrak{R}} \exp(-\mathfrak{R}^2/\bar{\mathfrak{R}}).$$

These equations describe the signal power fluctuation models of the raw data, $S(M)$, acquired by the imaging sensor. For the radar sensor adopted in this work, these well-established models describe an omnidirectional distribution of the signal intensity reflected from a landmark with multiple scatterers. An Exponential distribution is assumed for the radar noise signal, with a Ricean fluctuation model, $p(s|\Omega_m = \{\mu, \mathfrak{R}\}, m)$, adopted for the landmark signal. Since the intensity of the received signal is dependant on the viewing aspect, a Swerling I model, $p(\mathfrak{R}|\bar{\mathfrak{R}})$, is adopted to model the omnidirectional density of the SNR from a given landmark [Skolnik, 1982]. The proposed framework can naturally be adopted to any given distribution assumptions which can derive closed form likelihood equations such as eqn.(22).

As the assumed densities for radar systems are typically non-Gaussian as well as λ being a non-linear function of the observed data $S(M)$ (eqn.(22)) a particle approach is adopted to solve the recursion. Note the measurement likelihood estimate is valid for the radar sensor used in this work. By deriving a similar likelihood for other range measuring exteroceptive sensors such as underwater sonar and laser, the proposed algorithm can be generalized for use in multiple autonomous mapping applications.

V. PARTICLE FILTER IMPLEMENTATION

The objective of this filter is to propagate the posterior density of the joint density, $p(m_k, \lambda_k|z^k)$. Assume the prior, $p(m_{k-1}, \lambda_{k-1}|z^{k-1})$ can be represented by a set of weighted particles $\{x_{k-1}^{(i)}, w_{k-1}^{(i)}\}_{i=1}^N$ such that,

$$p(x_{k-1}|z^{k-1}) \approx \sum_{i=1}^N w_{k-1}^{(i)} \delta_{x_{k-1}^{(i)}}(x_{k-1})$$

where,

$$x_{k-1} = \begin{bmatrix} m_{k-1} \\ \lambda_{k-1} \end{bmatrix}$$

is the joint state containing the estimate on the map and the corresponding measurement likelihoods. Note that the measurement likelihood λ_k exists for both $m_k = 1$ (where it will be the landmark detection likelihood) and $m_k = 0$ (where it will be the false alarm likelihood).

To propagate the densities the standard particle filter recursion with resampling is followed,

$$x_k^{(i)} \sim q(x_k | x_{k-1}^{(i)}, z_k)$$

$$w_k^{(i)} = w_{k-1}^{(i)} \frac{p(z_k | x_k^{(i)}) p(x_k^{(i)} | x_{k-1}^{(i)})}{q(x_k^{(i)} | x_{k-1}^{(i)}, z_k)} \quad (23)$$

The transition likelihood $p(x_k^{(i)} | x_{k-1}^{(i)})$ describes the predicted state values and consists of the Markov time update described previously in section IV-D to propagate the occupancy random variable. This is a random particle set sampled from the previous posterior $p(x_{k-1} | z^{k-1})$ where the binary value of the m component is changed or remains fixed according to the probabilities set by the transition matrix, Π . A static time update for the measurement likelihood estimate (as it is assumed constant for each landmark) is used.

$$p(m' | z^{k-1}) \sim p(m_{k-1} | z^{k-1}, \Pi)$$

$$p(\lambda' | z^{k-1}) = p(\lambda_{k-1} | z^{k-1}) \quad (24)$$

The proposal likelihood $q(x_k | x_{k-1}^{(i)}, z_k)$ depends on whether the cell continues in its same state, i.e. during the Markov transition the cell value remains unchanged, or whether it changes state. In the case of the state remaining the same,

$$q(x_k^{(i)} | x_{k-1}^{(i)}, z_k) = p(x_k^{(i)} | x_{k-1}^{(i)}). \quad (25)$$

In the case of the state changing or a new detection, the data at time k is used to initialize the estimate on λ_k according to the measurement likelihood estimate algorithm outlined in the previous section IV-D. That is, the proposed detection likelihood is taken to be the estimated likelihood at that location using measurement data $S(M)$ through eqn.(22). Finally the likelihood used to weight the particles is obtained from the likelihood of a landmark being present in the cell which is also the same likelihood used by the detection algorithm (eqn.(15)) and is given by,

$$p(z_k | x_k^{(i)}) = \frac{p(s_r | m, \Omega_m)}{p(s_r | \bar{m}, \Omega_{\bar{m}})} \quad (26)$$

where s_r is the signal intensity at particle location $x^{(i)}$. The weighted particle set is then re-sampled. Estimates of the posterior occupancy and measurement likelihood can be extracted using the expected *a posteriori*,

$$\hat{x}_k = \sum_{i=1}^N w_k^{(i)} x^{(i)}. \quad (27)$$

VI. EXPERIMENTS

This section outlines experimental comparisons, using both real and synthetic data, of the proposed detection based RM algorithm with previous range likelihood approaches. The section shows superior mapping capabilities of the proposed method using metrics such as the sum total squared error, and quantitative comparisons of cell classification errors.

A. Dataset 1: Synthetic Data, Single Landmark

Simulated data was first generated using idealistic Gaussian fluctuating noise and a Gaussian fluctuating landmark of unknown mean intensity. The synthetic data is the same as used previously in section III-C. One hundred Monte Carlo trials were performed in which the occupancy posterior of each cell was propagated using the proposed algorithm with online DL estimation, and the standard occupancy algorithm where the DL is *a priori* assumed. For each trial, the assumed DL is increased by 0.01 to cover all possible values. As before (figure 3) the FAL is set at 0.1. Cells in which the posterior occupancy estimate is greater than 0.51 are declared occupied, and those less than 0.49 are declared empty. Figure 7 shows the percentage of false negatives (occupied cell declared empty) and false positives (empty cell declared occupied) for each trial. Note that when the assumed DL equals the false alarm likelihood, there is no information gained by either a detection or a non-detection thus the map remains in its initial state of $p(m_0)=0.5$. The percentage of false negatives remains high as expected when the DL is less than the FAL, but quickly drops to zero as the DL increases, thus showing that the proposed algorithm with DL filtering has a superior performance.

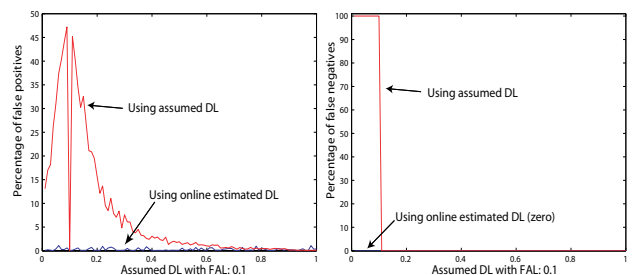


Fig. 7. Comparison of simulated mapping results using online DL estimation and the classical occupancy models where the likelihood is assumed. At pessimistically assumed DLs for the classic approach, the number of false positives and false negatives are dramatically greater than those using the proposed approach.

B. Dataset 2: The Carpark Environment

The section outlines a real-world application of the proposed method in an outdoor carpark environment. This environment contains numerous landmarks of varying dimension with *landmark dependant* detection likelihoods. Herein lies the inability to obtain the DLs for each object offline using training data, as the range of potential objects types (and hence DLs) in an outdoor environment makes it infeasible. A mobile platform, with mounted FMCW radar and LMS sensors, was remotely driven around the carpark. Four optical encoders record the input velocity to each wheel and a single-axis fibre optic gyroscope mounted over the rear axle gives estimates of the vehicle heading. With built-up surroundings, the GPS data acquired was not accurate enough to determine ground truth location. As the laser scans frequently obtained returns from the ground, automatic matching techniques failed

and therefore consecutive laser scans were manually matched to determine the true location of the vehicle at each update.

Laser data typically returns the range to the *first* landmark detected along the beam. For the case of the radar, a single beam can in fact contain information from multiple landmarks (see fig 5 for example) mainly due to the wider beamwidth ($\sim 1.8^\circ$ compared with $\sim 0.1^\circ$ for the laser) and the ability of the radar beam to penetrate some light foliage. The radar beam can penetrate and propagate into the trees and return information about multiple landmarks whereas the laser is limited to one return per beam. This optimistic approach therefore assumes that *every* measurement (detection and non-detection) along the entire beam is valid. That is, for each time step k , each peak in the data (under both the null and alternate detection hypotheses), is treated as a potential landmark, and no model of the sensor beam propagation properties is assumed. Detections registered over the test by a laser sensor and the radar sensor are shown in figure 8. Parameters for the radar detection OS-CFAR module (section IV-C and eqn.22) were chosen as $W = 40$, $K = 30$, and $P_{fa} = 1 \times 10^{-6}$. An overview of the carpark environment is shown in figure 9.

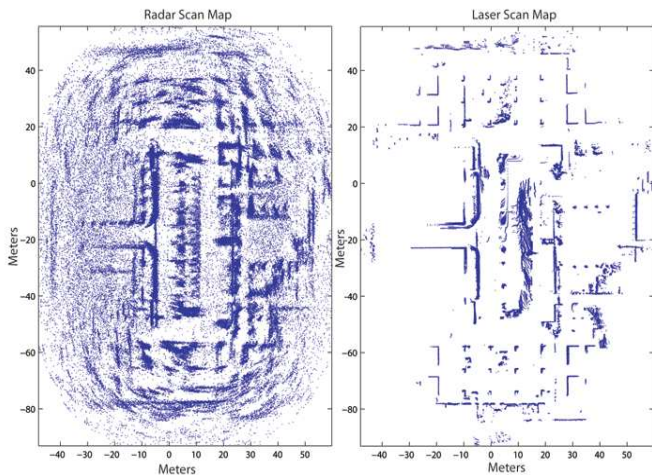


Fig. 8. Comparison of the detections reported by the radar for the entire carpark loop with those of the laser. Notice the high false alarm rate for the radar detections. False alarms (ground and grass detections) are also present in the laser data along the central region $(-45,5)$ to $(15,5)$.

Using the detection sequence depicted in figure 8, both detection and range likelihood approaches to the GBRM problem were implemented. Approximately 300 sensor scans were registered over the test, with the final posterior estimates of the map shown in figure 10. This shows mapping results from the proposed algorithm which estimates the detection likelihoods compared with previous approaches using assumed or range-based likelihoods [Thrun, 2003]. Visual inspection shows a reduction in false landmark declarations and an improved posterior map estimate. However, using the manually constructed ground truth map of the environment in figure 11, quantitative comparisons with previous approaches can be generated which highlight the advantages of the



Fig. 9. An overview of the testing ground from which the data presented in figures 8 and 10 was acquired. Also indicated is the path traversed by the vehicle. Only one car was present at time of data acquisition.

proposed method.

The error metric adopted for this work is a modification of the sum of the squared error [Martin and Moravec, 1996] over the estimated grid map, M_k , and the true map, M . For outdoor mapping applications, where there is a majority of empty cells as opposed to occupancy cells, the sum of squared error, which equally considers each (occupancy and empty) cell, was seen to result in an uninformative measure, especially in the presence of large landmark detection uncertainty. This is as a consequence of the total number of empty cells far exceeding the occupied cells. This paper therefore proposes an equally weighted (for both occupied and empty cells) error metric, referred to as the normalised averaged sum of the squared error (NASSE),

$$NASSE = 0.5 \left(\frac{1}{q_0} \sum_{i=0}^{q_0} (P(m_k^i | z^{i,k}, m^i = 1) - 1)^2 + \frac{1}{(q - q_0)} \sum_{i=q_0+1}^q (P(m_k^i | z^{i,k}, m^i = 0) - 0)^2 \right) \quad (28)$$

where, q is the total number of cells in the map, M , and q_0 is the number of ground truth occupied map cells. This metric presents a normalised error measure for use in environments of largely unequal numbers of occupied and empty cells. Figure 12 shows the sequential NASSE error for both approaches. It can be seen that the rate of monotonic error reduction of the proposed approach exceeds that of standard methods, with a reduced mapping error achieved in the final posterior map estimate. Figure 13 shows an error metric comparison, for the case of noisy vehicle control inputs. In this case the standard SSE metric shows monotonic error reduction where as the NASSE clearly shows mapping

inconsistency.

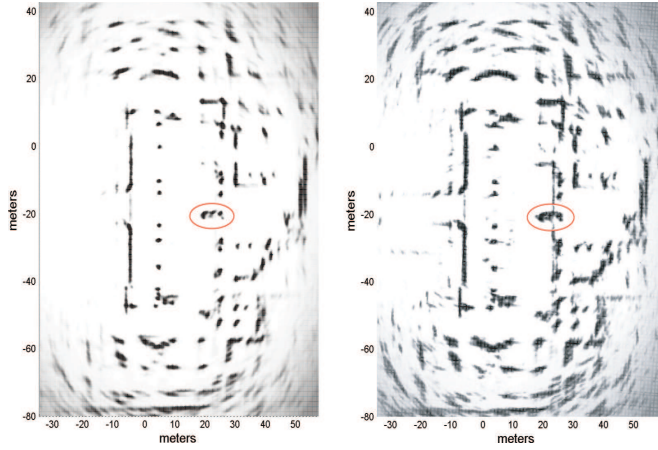


Fig. 10. The resulting occupancy maps produced by the proposed algorithm (left) and previous approaches with assumed likelihoods (right). Note the larger presence of falsely declared occupied cells using previous methods. Also highlighted is the only car present in the carpark during the time of the experiment.

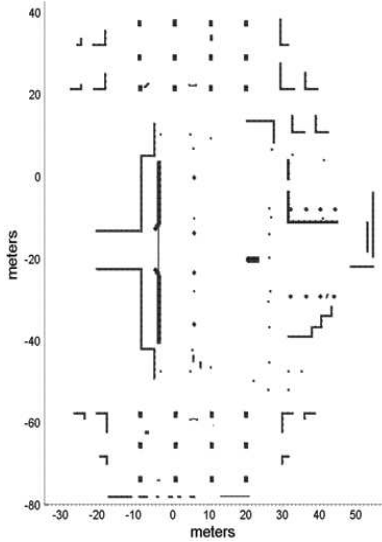


Fig. 11. Ground truth binary representation of the carpark testing environment. The map was manually constructed from observation of the testing ground shown in figure 9.

1) **Influence of Detection Module Parameters:** To generate detection measurements from the raw radar data (section IV-C), for both the range-likelihood and detection-likelihood methods implemented, an adaptive ordered statistics (OS) is adopted. Adaptive detectors use a sliding window of width, $W/2$, which samples local power readings and generates an estimate of the local noise in each range bin, r . Further parameters required to set the adaptive power threshold are the ‘K-value’, K , and the desired false alarm rate, P_{fa} . The latter parameter acts as a uniform scaling of the K^{th} ordered power sample in the window, and uniformly raises or lowers

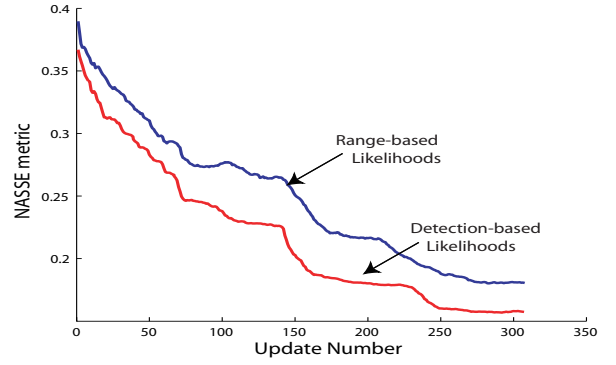


Fig. 12. Comparison of the NASSE metric between the estimated map posterior and the ground truth map. The result shows the monotonic reduction in the map error. For a given number of updates, the proposed approach out-performs that of previous methods which use range-based likelihoods.

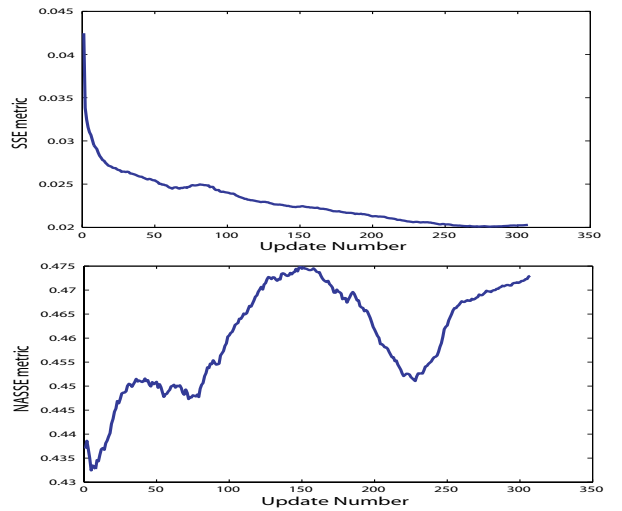


Fig. 13. Comparison of the error metrics for a loop with noise injected into the location estimates. This figure shows the susceptibility of the classical sum of squared error (SSE) metric, to maps containing unequal number of occupancy and empty cells. The NASSE error metric clearly indicates a non-converging map due to multiple missed landmarks, whereas the standard metric shows a monotonically decreasing error.

the adaptive power threshold calculated in the windowing function.

To synthesise an environment consisting primarily landmarks with low detection probability, the P_{fa} parameter of the detection algorithm can be set arbitrarily low (evident from figure 2). NASSE error plots for excessively low and high P_{fa} values are shown in figure 14. At extremely low P_{fa} , further advantages of the proposed algorithm are evident, since it explicitly considers the detection statistics, specifically the missed detection likelihoods, in the mapping recursion. For range-based methods, no range reading (as a result of a missed-detection), results in no range likelihood existing. Standard approaches therefore typically assign intu-

itive occupancy measurements in regions of no range reading [Thrun, 2003], [Elfes, 1989], [Foessel et al., 2001], [Konolige, 1997]. At high rates of false alarm, an increased rate of error reduction is evident with the proposed approach due to the formulation incorporating the detectors false alarm probability. This demonstrates the advantages of the proposed approach in the presence of both landmarks with low detection probability, and high rates of spurious detections.

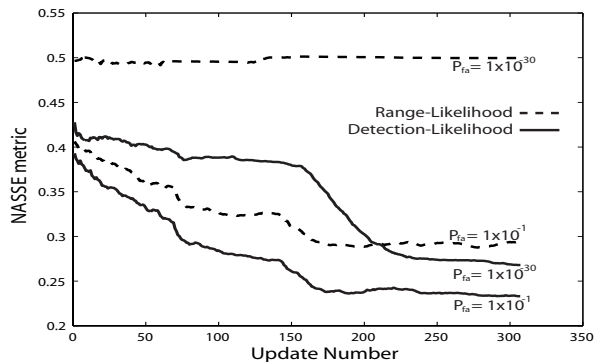


Fig. 14. Comparison of the NASSE metric in the carpark environment for very low detection probability, $P_{fa}=1 \times 10^{-30}$, and very high false alarm rate, $P_{fa}=1 \times 10^{-1}$.

The parameters, W , K , set the upper limit on the expected environmental landmark density along a single power-range spectrum (such as in figure 5) in the environment. As the estimate of the noise signal intensity is taken as the K^{th} ordered sample, with $W=40$ and $K=30$ and a range resolution of $25cm$ per range bin, allows for $(30/4)m$ to comprise of empty space and $(10/4)m$ (at most) to comprise of landmarks [Rohling, 1983]. The OS detection routine is quite robust to changing window size, however increased error at excessively small or large window sizes is evident, as shown in figure 15.

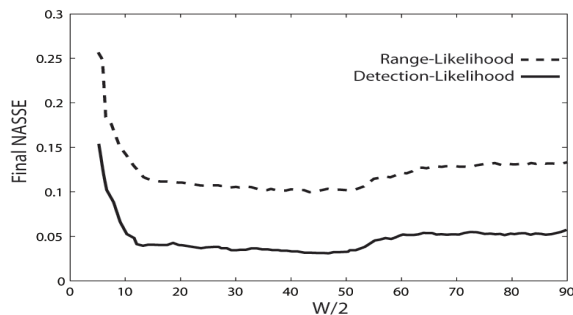


Fig. 15. NASSE for both approaches varying detection sliding window width, W , with $P_{fa}=1 \times 10^6$ and $K = 0.75 \times W$. For a given set of detector parameters, the proposed approach outperforms that of range-likelihood based methods, as the detection statistics are integrated into the mapping algorithm.

While these parameters may influence the detections registered by the imaging radar, this is common to any application adopting such a sensor. The results presented highlight that given any set of detector parameters, the proposed stochastic

mapping approach outperforms that of classical approaches, as it theoretically incorporates the resulting statistics, as a result of a given parameter choice, into the mapping recursion.

C. Dataset 3: The Campus Environment

The second dataset comprises an outdoor semi-urban environment within the university campus. Due to the practical challenges of obtaining a binary map ground truth from such an extensive environment, a high resolution undistorted (1 pixel/m) plan-view satellite image shown in figure 16 is used to provide map validation. The, approximately 500m long, path traversed by the vehicle is also shown. Figure 16 also shows the same image with superimposed hypothesised landmarks returned by the proposed algorithm. While quantification is challenging in such an environment, the results show good correlation with the satellite image, as numerous trees and buildings are clearly accurately registered. From comparison of the maps produced by the radar, using the proposed algorithm, and the laser in figure 17, the merits of radar as an outdoor exteroceptive sensor are evident. Due to the multiple-landmark-per-bearing-angle detection capability of the radar sensor, far more detail is apparent in its map than that of the single-landmark-per-bearing-angle laser.

VII. CONCLUSION

This paper presented a mapping algorithm for jointly estimating the occupancy variable along with its detection measurement likelihood. It showed that the measurement likelihood typically used in occupancy grid algorithms should in fact be modeled as a density function as opposed to a deterministic function, which is normally the case. By examining the measurement model and using signal detection theory, it is shown that the occupancy random variable can be calculated in closed form without the need of heuristic models. However, the measurement likelihood used in the occupancy posterior calculation is in itself an estimated entity, thus requiring a joint estimation frame work to propagate both the occupancy and measurement likelihood estimates.

The standard discrete Bayes estimation framework therefore no longer applies to the occupancy grid problem and a particle filter approach is proposed. Using Markov transitions, the effects of occlusions and the appearance of new landmarks in the region are integrated into the algorithm. Particle representations allow for the propagation of the measurement likelihoods (derived through a non-linear function of the sensor received intensity) subject to non-Gaussian noise. Weights for these particles are obtained from the likelihood ratio used by the detector. The resulting set of posterior particles is then resampled and the recursion is established.

This concept was demonstrated for an FMCW radar sensor which is typically used in an outdoor environment. The sensor gives access to unprocessed range data, allowing for custom landmark detectors to be applied. The framework then allows for the accurate assignment of map occupancy probabilities, irrespective of the hypothesis chosen by the detector. Mapping results were presented for loops in an outdoor carpark as

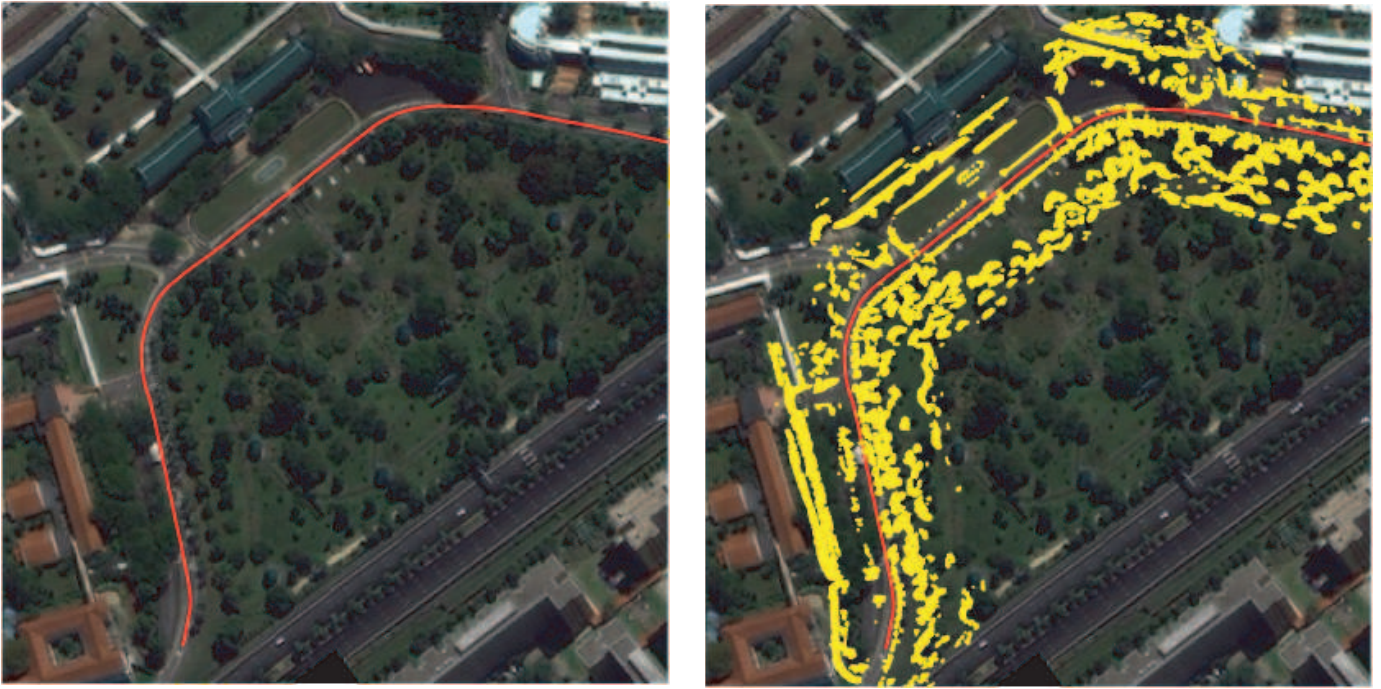


Fig. 16. A high resolution satellite image of the testing grounds within university campus. This provides some ground validation for the proposed mapping algorithm. The estimated vehicle path (obtained from the manually matching successive scans) is superimposed in red.

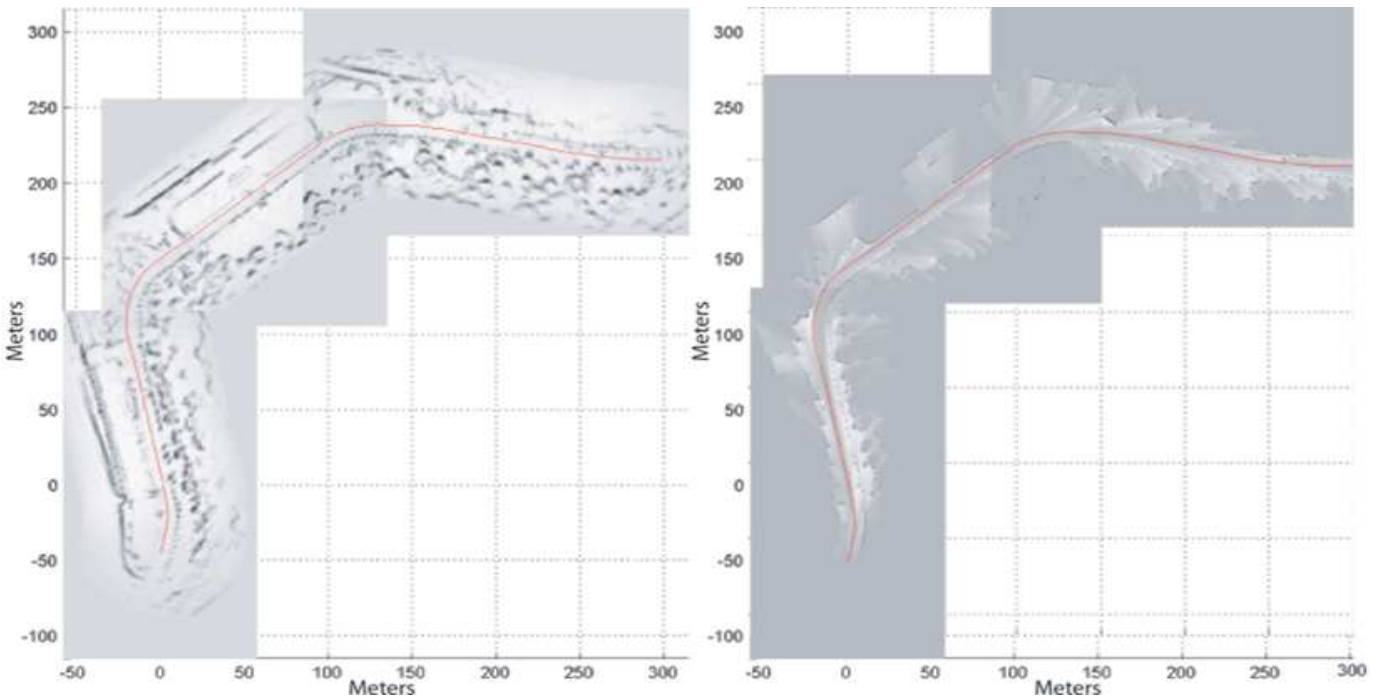


Fig. 17. The final posterior map estimates from a radar and laser sensor of the outdoor campus environment. Note the increased information content of the radar map, over that of the laser map, due to its ability to detection multiple landmarks at a single bearing angle.

well as within the university campus. Comparison with maps produced from previous approaches, ground-truth maps, laser occupancy maps as well as images show the merits of the proposed approach.

However, this work focused mainly on the online estimation of the detection likelihood and assumed the false alarm likelihood to be known. Due to the detection theory, thresholds are set using an *a priori* assumption on the distribution of the noise signal (as well as being assumed homogenous). Significant work needs to be carried out to accurately estimate the false alarm likelihood in regions of the map which deviate from the homogenous noise assumption, which can have drastic results for the occupancy posterior. Evidential modeling methods may be applied as there would be large uncertainty as to the true false alarm probability. This would further improve the mapping accuracy. Further work also would integrate the estimated detection likelihoods into data association decisions and SLAM algorithms as most hypothesis decision algorithms include detection likelihoods, which are again typically *a priori* assumed known. The consequences of such simplifications are currently under investigation.

ACKNOWLEDGEMENTS

This work was funded under the second author's AcRF Grant, RG 10/01, Singapore.

REFERENCES

- [Brooker et al., 2001] Brooker, G., Bishop, M., and Scheduling, S. (2001). Millimetre Waves for Robotics. In *Australian Conference for Robotics and Automation*, Sydney, Australia.
- [Clark and Dissanayake, 1999] Clark, S. and Dissanayake, G. (1999). Simultaneous Localisation and Map Building Using Millimetre Wave Radar to Extract Natural Features. In *Proceedings of the IEEE International Conference on Robotics and Automation*, pages 1316–1321, Michigan.
- [Clark and Durrant-Whyte, 1998] Clark, S. and Durrant-Whyte, H. (1998). Autonomous Land Navigation Using Millimeter Wave Radar. In *Proceedings of the IEEE International Conference on Robotics and Automation*, pages 3697–3702, Belgium.
- [Dissanayake et al., 2001] Dissanayake, G., Newman, P., Durrant-Whyte, H., Clark, S., and Csorba, M. (2001). A Solution to the Simultaneous Localization and Map Building (SLAM) Problem. *IEEE Transactions on Robotic and Automation*, 17(3):229–241.
- [Elfes, 1989] Elfes, A. (1989). *Occupancy Grids: A Probabilistic Framework for Robot Perception and Navigation*. PhD thesis, Robotics Institute, Carnegie Mellon University, Pittsburgh, PA.
- [Foessel et al., 2001] Foessel, A., Bares, J., and Whittaker, W. (2001). Three-Dimensional Map Building with MMW RADAR. In *Proceedings of the 3rd International Conference on Field and Service Robotics*, Helsinki, Finland.
- [Gandhi and Kassam, 1989] Gandhi, P. and Kassam, S. (1989). An Adaptive Order Statistic Constant False Alarm Detector. In *Proceedings of the IEEE International Conference on Systems Engineering*, pages 85–88, Ohio.
- [Grisetti et al., 2007] Grisetti, G., Stachniss, C., and Burgard, W. (2007). Improved Techniques for Grid Mapping With Rao-Blackwellized Particle Filters. *IEEE Transactions on Robotics*, 23(1):34–45.
- [Kay, 1998] Kay, S. (1998). *Fundamentals of Statistical Signal Processing, Vol II - Detection Theory*. Prentice Hall.
- [Kirubarajan and Bar-Shalom, 2001] Kirubarajan, T. and Bar-Shalom, Y. (2001). *Multisensor-Multitarget Statistics in Data Fusion Handbook*. CRC Press.
- [Konolige, 1997] Konolige, K. (1997). Improved Occupancy Grids for Map Building. *Autonomous Robots*, 4(4):351–367.
- [Leonard and Durrant-Whyte, 1990] Leonard, J. and Durrant-Whyte, H. (1990). Dynamic Map Building for an Autonomous Mobile Robot. In *Proceedings of the IEEE International Workshop on Intelligent Robots and Systems*, pages 89–96, Ibaraki, Japan.
- [Lu and Miliotis, 1997] Lu, F. and Miliotis, E. (1997). Robot Pose Estimation in Unknown Environments by Matching 2D Range Scans. *Journal of Intelligent and Robotic Systems*, 18(3):249–275.
- [Majumder, 2001] Majumder, S. (2001). *Sensor Fusion and Feature Based Navigation for Subsea Robots*. PhD thesis, The University of Sydney.
- [Makarsov and Durrant-Whyte, 1995] Makarsov, D. and Durrant-Whyte, H. (1995). Mobile Vehicle Navigation in Unknown Environments: A Multiple Hypothesis Approach. *IEE Proceedings of Control Theory Applications*, 142(4):385–400.
- [Martin and Moravec, 1996] Martin, M. and Moravec, H. (1996). Robot Evidence Grids. Technical Report CMU-RI-TR-96-06, Carnegie Mellon University, Pittsburgh.
- [Montemerlo et al., 2003] Montemerlo, M., Thrun, S., Koller, D., and Wegbreit, B. (2003). FastSLAM 2.0: An Improved Particle Filtering Algorithm for Simultaneous Localization and Mapping that Provably Converges. In *Proceedings of the 18th International Joint Conference on Artificial Intelligence*, pages 1151–1156, CA.
- [Moravec and Elfes, 1985] Moravec, H. and Elfes, A. (1985). High Resolution Maps from Wide Angle Sonar. In *Proceedings of the IEEE International Conference on Robotics and Automation*, pages 116–121, New Jersey.
- [Mullane et al., 2006] Mullane, J., Adams, M., and Wijesoma, W. (2006). Evidential versus Bayesian Estimation for Radar Map Building. In *Proceedings of the 9th IEEE International Conference on Control, Automation, Robotics and Vision (ICARCV 2006)*, Singapore.
- [Mullane et al., 2007] Mullane, J., Jose, E., Adams, M., and Wijesoma, W. (2007). Including Probabilistic Target Detection Attributes into Map Representations. *International Journal of Robotics and Autonomous Systems*, 55(1):72–85.
- [Ribas et al., 2007] Ribas, D., Ridao, P., Tardos, J., and Niera, J. (2007). Underwater SLAM in a Marina Environment. In *Proceedings of the IEEE/RSJ International Conference on Intelligent Robots and Systems*, San Diego, CA.
- [Rohling, 1983] Rohling, H. (1983). Radar CFAR Thresholding in Clutter and Multiple Target Situations. *IEEE Transactions on Aerospace and Electronic Systems*, 19(4):608–621.
- [Rohling and Mende, 1996] Rohling, H. and Mende, R. (1996). OS CFAR Performance in a 77 GHz Radar Sensor for Car Applications. In *Proceedings of the CIE International Conference of Radar*, pages 109–114.
- [Skolnik, 1982] Skolnik, M. (1982). *Introduction to Radar Systems*. McGraw Hill, New York.
- [Smith et al., 1987] Smith, R., Self, M., and Cheeseman, P. (1987). A Stochastic Map for Uncertain Spatial Relationships. In *The Fourth International Symposium of Robotics Research*, pages 467–474.
- [Thrun, 2003] Thrun, S. (2003). Learning Occupancy Grids with Forward Models. *Autonomous Robots*, 15(2):111–127.
- [Thrun et al., 2005] Thrun, S., Burgard, W., and Fox, D. (2005). *Probabilistic Robotics*. MIT Press, Cambridge, MA.
- [Wijesoma et al., 2006] Wijesoma, W., Perera, L., and Adams, M. (2006). Toward Multidimensional Assignment Data Association in Robot Localization and Mapping. *IEEE Transactions on Robotics*, 22(2):350–365.
- [Williams, 2001] Williams, S. (2001). *Efficient Solutions to Autonomous Mapping and Navigation Problems*. PhD thesis, Australian Centre for Field Robotics, University of Sydney.